

# Experimental measurement of *n*-pentane flame speeds at elevated pressures and temperatures

A. P. Kelley, A. J. Smallbone, D. L. Zhu, C. K. Law\*

*Department of Mechanical and Aerospace Engineering  
Princeton University, Princeton, NJ, 08544*

---

## Abstract

An existing high- and constant-pressure, double-chamber apparatus designed to measure the laminar flame speeds of gaseous fuels has been upgraded to accommodate volatile liquid fuels up to 30 atm. Specifically, the apparatus can be electrically heated to the temperature range of 80°C to ensure complete vaporization of the liquid fuel. The design involves injecting the liquid fuel via a syringe into a heated injection chamber with the resulting fuel vapor circulated into the combustion chamber. Heated gases are then introduced into the chamber to create the desired mixture composition and pressure. Equivalence ratios were checked using gas chromatograph analysis. The laminar flame speed and Markstein length are extracted from the flame motion using a nonlinear extrapolation expression to ensure fidelity of the extrapolation. Results are reported for *n*-pentane/air mixtures at 1, 2, 5, and 10 atmospheres and compared with calculations using a mechanism recently developed for the oxidation of *n*-alkanes up to *n*-dodecane. The onset of cellular instabilities was observed at higher pressures and the critical Péclet numbers at the state of formation are reported.

---

## 1. Introduction

As computational capability continues to increase, simulation of the combustion behavior of realistic fuels is becoming increasingly possible, leading to the recent interest in the development of the oxidation mechanisms of high molecular weight hydrocarbons [1]. The fidelity of these mechanisms are typically validated against experimental measurements including ignition delay, flow and stirred reactors, and laminar flame speeds.

For high molecular weight hydrocarbons, there exist few high fidelity experimental measurements of laminar flame speeds which can be compared with the predictions of chemical kinetic models. Davis and Law [2–5] determined the flame speeds of many hydrocarbon isomers up to C<sub>8</sub> at atmospheric pressure. Additional laminar flame speed measurements have been conducted by Egolfopoulos *et al.* [6] which determined the flame speed for *n*-alkanes up to *n*-dodecane, also at atmospheric pressure.

Although atmospheric flame speed measurements are useful, three-body recombination reactions increase in frequency at high pressures [7], thereby imposing a distinctive, nonlinear pressure effect on the overall reaction response. As such, it is essential to incorporate pressure variation in the target matrix when developing reaction mechanisms. Furthermore, internal combustion engines operate on the principle of high pressure combustion, necessitating the measurement of flame speeds at elevated pressures.

To date, high-pressure measurements of the flame speed of liquid fuels are limited, notably those of *n*-heptane [8–10], *iso*-octane [9–11], and the aromatics [12]. However, high-pressure laminar flame speeds for many other liquid fuels of importance to chemical kinetic modeling have yet to be measured. The reason for the paucity of the data on high molecular weight hydrocarbons at high pressures is the difficulty in the experimentation. For example, these fuels typically have low vapor pressures – necessitating that the experiments be carried out at elevated temperatures to ensure gasification of the liquid. The simultaneous requirement of high pressure and temperature impose severe challenge in the experimental design. Furthermore, when the counterflow configuration is used, the flow under such conditions tends to be turbulent. Finally, flame front cellular instabilities tend to develop over the flame surface at high pressures, obviating the relevance of the flame surface morphology based on which the flame speed is defined.

## 2. Objectives

Our objective in the current study is to design an experimental apparatus that will allow the measurement of high-pressure flame speeds for high molecular weight fuels which are typically in a liquid state at room pressure and temperature. These data will then be compared with the calculated values in order to scrutinize the performance of the reaction mechanisms used.

In order to achieve this objective, we have adopted the outwardly propagating flame, as this method has proven to be the most successful for high-pressure flame speed measurements *e.g.* [9, 11, 13–20]. To achieve results of high fidelity, the experiment must be conducted at nearly constant pressure, must

---

\*Corresponding author: cklaw@princeton.edu  
Associated Web site: <http://pcl.princeton.edu>  
Proceedings of the 6th U.S. National Combustion Meeting

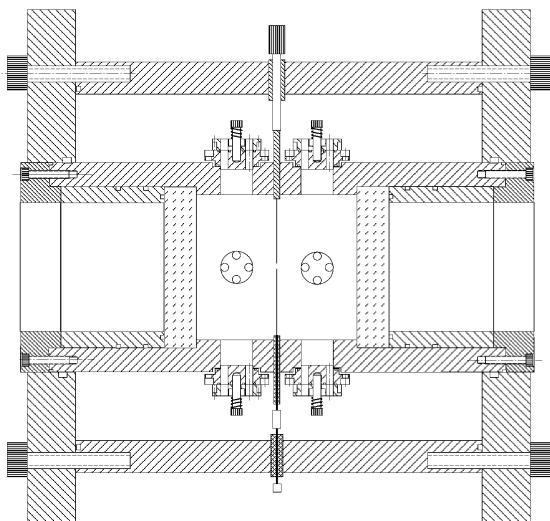


Figure 1: Schematic showing cutout of inner and outer chamber.

have optical access to ensure that the flame surface is spherical and free of instabilities, and must properly account for the effects of stretch. Furthermore, in order to use liquid fuels, the entire apparatus must be heated to ensure that the liquid fuels remain in the gas phase.

We have therefore designed an experimental apparatus which addresses each of these issues. To validate the measurements of the apparatus, we shall present measurements of the flame speed of *n*-pentane at atmospheric pressure and room temperature, as well as measurements at elevated temperatures and pressures. These data represent the first *n*-pentane flame speed measurements at high pressures. Additionally, we will present the radius at which the onset of cellular instability occurred in rich high-pressure experiments.

In the next section, we will discuss the experimental design and limitations. We will then discuss the experimental procedure, the extrapolation of the laminar flame speed, and our results.

### 3. Experimental Design

Conceptually, the design of the apparatus is similar to our previous design for the high-pressure flame propagation at room temperature [21]. The apparatus is a double chamber vessel with one cylindrical chamber radially surrounding the other, as shown schematically in Fig. 1. The experiment was designed with the goal of allowing a nearly constant pressure spherical flame to propagate and be visually recorded at pressures up to 30 atmospheres. The experiment additionally required uniform heating of the test gas in order to ensure that the liquid fuels remained in the gas phase.

#### 3.1. Inner Chamber

The inner chamber consists of a cylindrical experimental test section (I.D. 4.5", O.D. 6.5", length 5"). The two ends of the chamber are sealed with 1" thick, 5" diameter, quartz windows

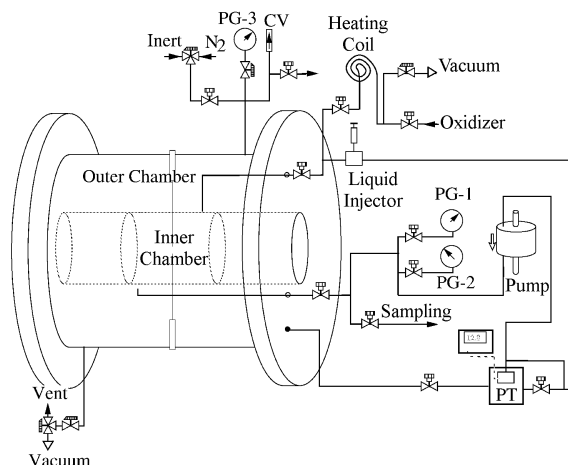


Figure 2: Plumbing diagram for experimental vessel. CV: Check Valve (safety for over-pressurization), PG: Pressure Gauge, PT: Pressure Transducer.

which allow optical access. Four fans of 2.7" diameter are located at its walls and are driven by motors enclosed in the outer chamber. These fans are radially located at 90° to one another and are centered axially in the chamber. The fans are omitted from Fig. 1 for clarity.

The walls of the inner chamber are fitted with a total of 32 holes of 0.221 inch diameter. The holes are arranged as eight sets of four. Each set of four holes has a circular disk which sits above the holes. The disk has a set of matching holes and can either seal the inner chamber walls via four buta-n o-rings, or rotate 45° to align the holes and connect the inner and outer chambers.

The chamber has two 1/4" stainless steel tubes connected to it. The tubes form a closed loop which passes outside of the outer chamber as shown in Fig. 2. Along the closed loop are two valves which allow the loop to be sealed from the inner chamber prior to ignition. The loop has a series of components: two pressure gauges, a one-way pump, a pressure transducer, a gas sampling port, a liquid injection port, and a gas injection port.

The pressure gauges are manufactured by CECComp Electronics and measure the pressure from 0-15 *psia* and 0-100 *psia* respectively. The one-way pump operates at 60 *Hz* and has a flow rate of approximately 0.85 *L/min*. The pressure transducer measures the pressure differential between the inner and outer chambers. The gas sampling port collects samples of the unburned gas for gas chromatograph analysis.

The liquid injection port has a septum which allows syringe injection of the liquid fuel. The port has a quartz window onto which the liquid is injected to allow visual inspection of the injection and subsequent vaporization. A K-type thermocouple was used to monitor the temperature on the inner surface of the quartz window.

Three K-type thermocouples are placed to ensure that the temperature of the inner chamber is uniform. One thermocouple is located in the gas of the inner chamber, near the wall, and the remaining thermocouples are located on the top and bottom

surfaces of the chamber wall.

Two electrodes are located inside of the chamber. They are vertically oriented and centered axially. The electrodes have a gap which is variable by means of a micrometer. The top electrode is grounded, whilst a high voltage is applied to the bottom electrode resulting in a controlled spark.

The total volume of the gas in the chamber and the attached plumbing loop was experimentally determined by injecting a known volume of air into the chamber and measuring the pressure rise. The volume was determined to be 1.91 liters with an uncertainty of 1.4%.

### 3.2. Outer Chamber

The outer chamber consists of a cylindrical vessel (I.D. 10.75", O.D. 12.75", length 12.7") with four attachments in which the motors for the inner chamber fans are encased.

Attached to the outer chamber is a gas injection port which allows a mixture of inert gases to be injected. Additionally, a high pressure gauge manufactured by CECComp Electronics measures the chamber pressure up to 1000 *psig*. A pressure tap runs from the outer chamber to the pressure transducer which measures the pressure differential between the inner and outer chambers. The total gas volume of the outer chamber was experimentally determined to be roughly 13 liters.

The temperature of the outer chamber is monitored via four K-type thermocouples, with three of them monitoring wall temperature on the top, bottom, and end of the outer chamber cylinder, and the remaining one measuring the gas temperature in the outer chamber.

### 3.3. Heating

The vessel is heated using silicon rubber heat sheets with adhesive backing. The heat sheets have a maximum output of 10 *W/in<sup>2</sup>*. The temperature is maintained in four different zones using thermocouple controllers (Fuji Electric Systems Model PXR3). The four zones which are controlled are the ends of the outer chamber, the radial outside of the outer chamber, the injection port, and the one-way pump which have 600 *W*, 1680 *W*, 40 *W*, and 120 *W* of heating respectively available.

Due to inevitable heat loss from the outer chamber, the temperature of the outer chamber must be slightly lower than the desired inner chamber temperature to maintain the proper temperature gradient. The outer chamber is therefore maintained at 77.2°C, with a corresponding inner chamber temperature of 80°C.

After the vessel has reached a steady state temperature, the three temperature readings for the inner chamber agree to within 1°C, ensuring that the entire inner chamber is of nearly uniform temperature. Such a uniform temperature is required to ensure that there are no currents generated by buoyant forces which could disturb the measurement of the flame speed.

The plumbing is heated via a 520 *W* tape heater manufactured by Omega. The temperature is monitored via a K-type thermocouple attached to the outside of the plumbing. The temperature of the plumbing is maintained slightly above the desired inner chamber temperature to ensure that condensation

does not occur within the tubing. Due to the large heat capacity of the chamber relative to the gas, slightly raising the temperature of the gas while it is in the plumbing does not result in a change in temperature of the gas in the inner chamber.

Prior to the gas entering the gas injection port of the inner chamber, it must pass through a heated coil. The coil is heated via an 18 *W* silicon heater which raises the gas temperature above the temperature in the inner chamber. This is done to ensure that the incoming gas does not cool the gaseous fuel and cause condensation.

The entire experiment is insulated using a combination of melamine foam, silicon insulation, and Nomex wrap. Two safety interlocks are incorporated into the heating control system: a smoke detector and a thermal fuse.

### 3.4. Visualization

The flame surface is visualized using a Schlieren system that allows visualization of the density gradient and thus temperature gradient in the inner chamber. The Schlieren system consists of a 100 *W* mercury lamp (Newport Model 66902) which is focused to a point and passes through a small hole to ensure that the light source closely represents a point source. The light then passes through an achromatic plano-convex lens of focal length 250 *mm* with a diameter of 3 inches which creates a parallel light source. The parallel light passes through the inner chamber and then another plano-convex lens where it is focused. At the focal point, an adjustable iris is used to create a pin-hole Schlieren effect.

The resulting image is recorded via a Vision Research Phantom v7.0 high speed camera with maximum resolution of 800 × 600 pixels and maximum speed of 150,000 *frames/sec*. During typical experiments, the camera resolution is set to 700 × 350 pixels running at 8,000 *frames/sec*. The spatial resolution of the camera corresponds to approximately 0.1 *mm/pixel*.

### 3.5. Ignition Source

The electrodes are energized by discharging a 33 $\mu$ *F* capacitor through an ignition coil. The ignition coil increases the voltage which is then discharged across the electrodes resulting in a spark. The discharge occurs in approximately 1 $\mu$ *s*. The capacitor is charged with a voltage difference of up to 170 *V* across it. Therefore, the theoretical maximum spark energy is approximately 500 *mJ*. This is an overestimate due to inevitable losses in the electrical system.

## 4. Experimental Procedures

The vessel is allowed at least three hours subsequent to turning on the heaters to reach a uniform and steady temperature prior to beginning any experiments.

The entire vessel is first vacuumed, then twice filled with air and vacuumed to remove any gases from previous experiments. With the entire vessel vacuumed, the inner and outer chambers are separated by means of rotating the disks which seal the inner chamber from the outer chamber.

To achieve a desired equivalence ratio, the volume of fuel necessary is calculated using the ideal gas law, knowing the inner chamber volume, temperature, and the density of the liquid fuel. The fuel is injected using a single injection from Hamilton Gastight SampleLock syringes of varying sizes. The fuel is injected through a septum into the heated injection port. The liquid fuel is allowed to vaporize which typically takes a few seconds, depending on the volume of fuel injected. Vaporization is ensured by three means. First, a quartz window located on the liquid injection port allows visual confirmation of complete vaporization. Additionally, a thermocouple located on the quartz window is monitored until the quartz window had returned to the operating temperature before proceeding. The partial pressure of the fuel can then be determined via a pressure gauge and compared with the expected partial pressure based on the volume of fuel injected.

Preheated gases are then introduced into the inner chamber at a slow rate until the desired experimental pressure is reached. Typically, these gases consist of a premixed certified cylinder of oxygen and inert gas. For the current study, the preheated gases were a mixture of 21% O<sub>2</sub> with the balance being N<sub>2</sub>. This mixture allows for easy modeling of the experimental results and eliminates the inconsistencies of relative component concentrations in compressed air.

Simultaneous to the filling of the inner chamber with gases, the outer chamber is filled with a mixture of inert gases. For this particular study, a mixture of nitrogen and argon was used. The mixture is such that the average molecular weight of the gases in the outer chamber matches that of the inner chamber to minimize buoyancy of the gases. The pressure differential between the two chambers is kept minimal during the filling process to minimize any small leaks between the inner and outer chambers. This pressure differential is continuously monitored via the pressure transducer.

Once the final pressure is reached, the one-way pump and the fans in the inner chamber are turned on. The pump serves to ensure complete mixing of the gas in the inner chamber with the gas in the plumbing. The fans ensure homogeneity of the mixture. The gases are allowed to mix for 5 minutes which corresponds to pumping the entire volume of the inner chamber through the plumbing twice to ensure complete mixing. It was found that even small pockets of gas which were not completely mixed could change the equivalence ratio significantly due to the small amount of fuel relative to the oxidizer.

Prior to ignition the plumbing is sealed from the inner chamber via a series of valves. This protects the equipment from the high temperature of combustion. The mixture is then ignited and simultaneously the disks on the wall of the inner chamber are rotated to connect the inner chamber to the outer chamber and the camera is triggered to record. A spherical flame subsequently propagates from the spark ignition source to the walls of the inner chamber where it is quenched by the inert gases. The pressure is nearly constant during the propagation due to the large volume of the total gas in the inner and outer chambers. Due to the large relative fraction of inert gases, the resulting pressure rise after the experiment is minimal, ensuring that the structural integrity of the optical windows is not compro-

mised.

The flame is imaged using the high speed camera and Schlieren imaging technique. The images are subsequently analyzed to determine the flame radius as a function of time. These data are used to determine the unstretched laminar flame speed.

Since flame speed is highly sensitive to small errors in the quantities of injected fuel (at 1 atmosphere, changing the volume of fuel injected by 14  $\mu$ L changes the equivalence ratio by 0.1), the equivalence ratio was checked using three methods to ensure robustness. Although the equivalence ratio is determined by the volume of fuel injected and checked by the partial pressure rise after fuel injection, a third check of the equivalence ratio is conducted to ensure its accuracy. Subsequent to flame propagation, but prior to opening the valves connecting the plumbing to the inner chamber, a sample of the unburned gas is taken from the plumbing lines. The samples are then run through an SRI 8610C Gas Chromatograph equipped with a flame ionization detector. The detector was calibrated using a calibration standard obtained from Matheson Tri-Gas with 1000 PPM of *n*-alkanes from C<sub>1</sub> to C<sub>6</sub>. Measurements of the equivalence ratio using the gas chromatograph were within the random error of 2% calculated from error analysis.

## 5. Data Analysis

The extrapolation of the laminar flame speed has proven to be a relatively difficult task, requiring considerations of the ignition transient [22], chamber confinement effects [23], and the intrinsic nonlinear variation of the flame speed with the stretch rate [24]. As such, a brief description of the extrapolation procedure allowing for the nonlinear stretch effect is given in Appendix A.

We have used the nonlinear relationship of equation 6 for regression of our experimental data. This regression yielded the unstretched downstream flame speed which was then converted to an unstretched upstream flame speed by use of the continuity equation and associated density jump across the flame. Additionally, the regression determines the downstream Markstein length,  $L_b$ .

Data used for regression were typically taken from a range of 1.0 to 1.8 *cm* in radius. This range was determined experimentally to remove the transient influence of ignition and the influence of the chamber boundary which confines the motion of the unburned gas. A more detailed discussion may be found in Appendix B

## 6. Results and Discussion

To validate the apparatus, *n*-pentane was chosen as a representative liquid fuel. The vapor pressure of *n*-pentane is such that it does not require heating for low pressure measurements, therefore allowing comparison of 1 *atm* experiments with measurements reported in the literature.

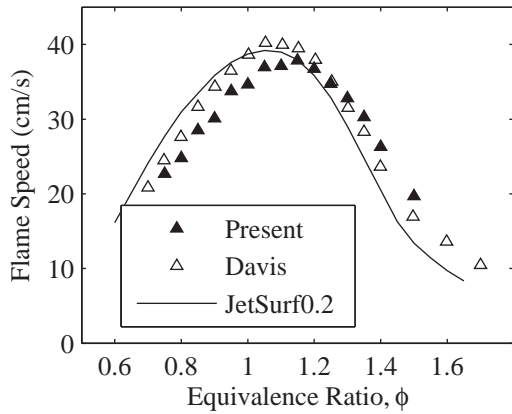


Figure 3: Comparison of 1 atm,  $T_u = 25^\circ\text{C}$  flame speed measurements with those of Davis [3]. Calculation of JetSurf0.2 [1]: solid line.

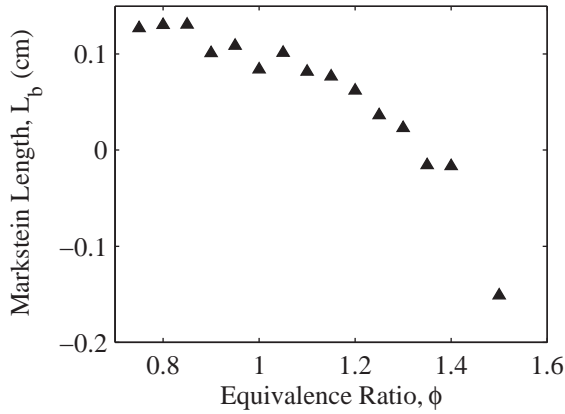


Figure 4: Markstein lengths of *n*-pentane/air experiments for  $T_u = 25^\circ\text{C}$  and initial pressure of 1 atm.

### 6.1. Room Temperature and Pressure

As shown in Fig. 3, one atmosphere flame speeds were measured with an initial temperature of  $25^\circ\text{C}$ . The resulting flame speeds are compared with those measured by Davis [3] using the counterflow. It is seen that the data agree fairly well with Davis, however the lean experimental data appears to be slightly lower.

In both Davis's experiments and the results shown presently, gas chromatograph analysis was used to ensure that the equivalence ratios were correct. The experimental errors associated with Davis's and the present measurement are on the order of 1 to 2 cm/s. However, the reason for discrepancy between the two data sets is uncertain.

Figure 4 plots the Markstein lengths associated with the flame speed measurements in Fig. 3. We see that both lean and rich mixtures have a relatively large value of the Markstein length. Mixtures near  $\phi = 1.30$  were seen to have vanishing Markstein length, implying that these mixtures are nearly equidiffusive and therefore the Lewis number is near unity.

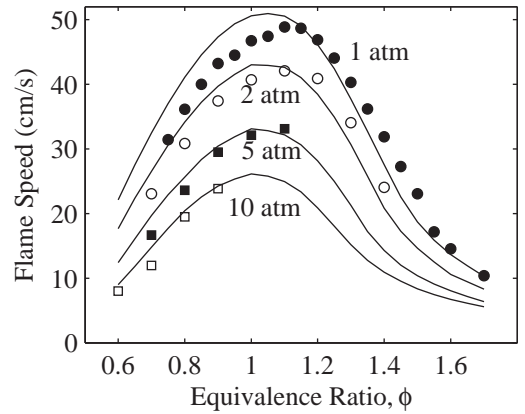


Figure 5: Flame speed of *n*-pentane/air experiments with  $T_u = 80^\circ\text{C}$ . Calculation of JetSurf0.2 [1]: solid lines.

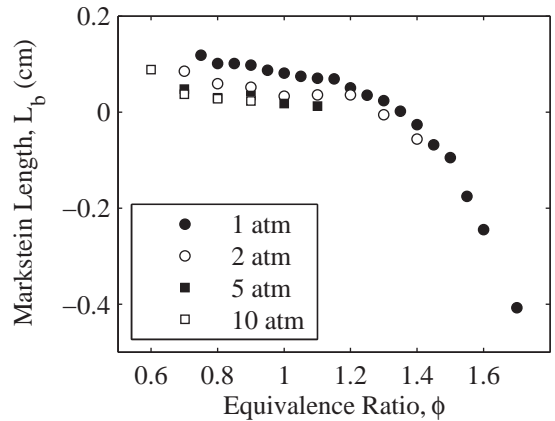


Figure 6: Markstein lengths of *n*-pentane/air experiments for  $T_u = 80^\circ\text{C}$ .

### 6.2. Elevated Temperature and Pressure

Measurements were also taken for *n*-pentane/air mixtures at elevated pressures and temperatures. An elevated temperature of  $80^\circ\text{C}$  was chosen such that similar experiments with higher molecular weight hydrocarbons could be conducted and readily compared in later work. The measurements of the flame speed and associated Markstein lengths are shown in Figs. 5 and 6 respectively.

We see that the flame speed decreases with increasing pressure, as is expected. However, in Fig. 7 we see that the mass flux increases with pressure. The flame speed appears to peak at  $\phi \approx 1.10$  for all pressures. It may be noted that the Markstein length for 1 and 2 atmosphere experiments appeared to vanish around  $\phi = 1.30$  indicating a nearly diffusionally neutral mixture and hence  $Le \approx 1$ , in agreement with the results for room temperature experiments. Additionally, it may be seen that the Markstein length decreases with increasing pressure because of the correspondingly reduced flame thickness and thereby diffusion effects.

For each pressure, the lean limit of the experimentation was such that the ignition energy available was not sufficient to drive the flame beyond the critical radius required for success-

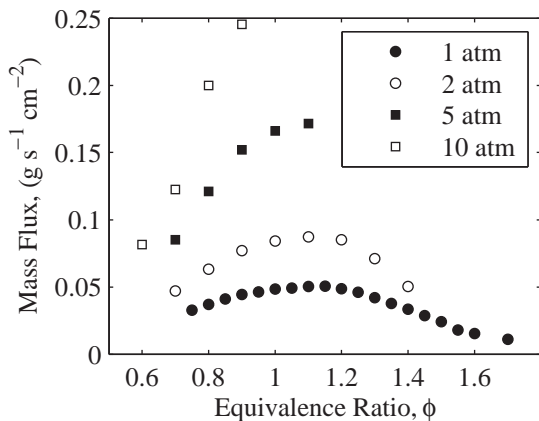


Figure 7: Mass flux of *n*-pentane/air experiments for  $T_u = 80^\circ\text{C}$ .

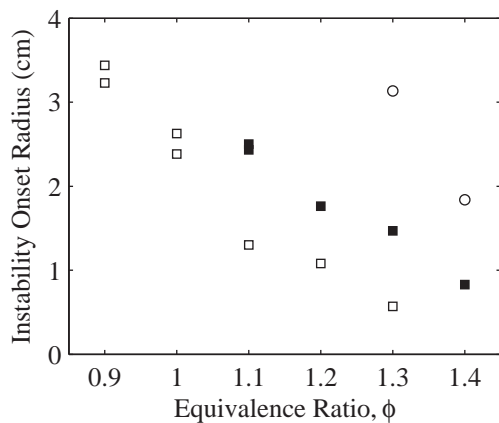


Figure 8: Onset radius of small scale cellular instability for *n*-pentane/air flames with  $T_u = 80^\circ\text{C}$ . open circle: 2 atm, filled square: 5 atm, open square: 10 atm.

ful flame initiation [13]. The limit for rich experimentation was determined by the propensity of the flames to become cellularly unstable, for the 2, 5 and 10 atmosphere experiments. For the 1 atmosphere experiments, the rich limit was a result of buoyancy of the flame. These cellular instabilities caused the flame speed to rapidly increase and prevented the measurement of the laminar flame speed.

### 6.3. Instabilities

As pressure was increased, instabilities began to form, particularly for rich mixtures. Therefore, these experiments were not used for the measurement of the laminar flame speed, but were studied to determine the onset of instability. Some large-scale cracks might appear near to the moment of spark ignition. However, once the flame grew to a certain size, it would quickly undergo a transition to small-scale cellular instabilities covering its entire surface, as described in Ref. [25]. This instant is defined as the critical state of instability.

Experiments were conducted to determine the radius at which the small wavelength, uniformly distributed, instabilities formed. Figure 8 plots the radius at which the small scale instabilities were seen to begin. Since *n*-pentane/air is diffusively

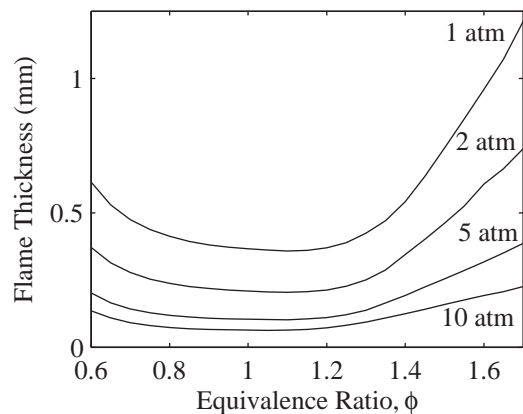


Figure 9: Flame thickness calculated using Eq. 1 and the chemical kinetic mechanism of Ref. [1] for *n*-pentane/air flames with  $T_u = 80^\circ\text{C}$  at various pressures.

unstable for rich mixtures, and since the positive stretch associated with the expanding spherical flame tends to suppress the diffusion cells and its intensity decreases with increasing flame radius, the results show the reasonable trend that the flame becomes unstable at smaller flame radius with increasing equivalence ratio. Furthermore, since the flame tends to be hydrodynamically unstable when it is thinner, and the flame thickness tends to decrease with increasing pressure, the results of Figure 8, that the flame tends to be more unstable at higher pressures, occurring at smaller radii, are also reasonable.

A more systematic indication of the propensity to destabilize is through the Péclet number for the onset of instability, defined as the ratio of the physical onset radius to the corresponding flame thickness [26]. To conduct such a comparison, the flame thickness was calculated using the gradient method as discussed in Ref. [27],

$$\ell_T = \frac{T_b^o - T_u}{(dT/dx)_{max}} \quad (1)$$

where  $\ell_T$  is the flame thickness,  $T_b^o$  the adiabatic flame temperature,  $T_u$  the unburned gas temperature, and  $x$  the coordinate normal to the flame surface. Figure 9 plots the flame thickness calculated using Eq. 1 and the chemical kinetic mechanism Jet-Surf0.2 described in Ref. [1].

Using these data, the Péclet number for the onset of small scale cellular instability is plotted in Fig. 10. The Péclet number at which instabilities formed is seen to have a roughly linear relationship which holds for all pressures tested. This is consistent with the results of Jomaas *et al.* [25] for non-equidiffusive mixtures. Additionally Jomaas *et al.* determined that the Péclet number for instability onset of diffusively neutral mixtures was roughly 350. From Fig. 10, it is seen that this corresponds to slightly rich mixtures. This roughly agrees with the measurement of a diffusively neutral mixture based on vanishing Markstein length, as seen in Fig. 6.

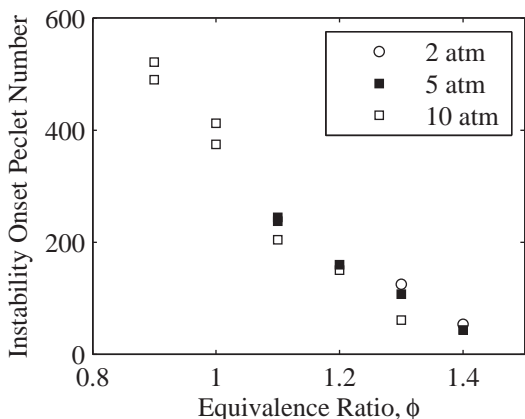


Figure 10: Critical Péclet numbers for transition to small scale cellular instability for *n*-pentane/air flames with  $T_u = 80^\circ\text{C}$  at various pressures.

#### 6.4. Comparison with Chemical Kinetic Mechanism

JetSurf0.2 [1] is a recently developed chemical kinetic mechanism for the high temperature oxidation of *n*-alkanes from  $\text{C}_5$  to  $\text{C}_{12}$ , and was used to calculate the laminar flame speeds of *n*-pentane/air for comparison with the experimental results. The calculations were conducted using the Chemkin program Premix. The results of these calculations are given in Figs. 3 and 5.

From Fig. 3 and 5 we see that the predictions of the mechanism show fairly good qualitative agreement with the experimental data. However, disagreement is most apparent for experiments conducted at 1 atmosphere of pressure. For both room temperature and elevated temperature experiments, we see that the mechanism slightly over-predicts the flame speed for lean mixtures, while the agreement is better for rich mixtures. The agreement overall improves for the elevated pressure results. Additionally, the experimental results suggest a peak flame speed that is slightly richer than the prediction of the mechanism.

## 7. Conclusions

A new experimental device was designed and built to experimentally determine the laminar flame speeds of liquid hydrocarbon fuels at elevated pressures and temperatures. The experiment can accommodate initial temperatures up to  $80^\circ\text{C}$  and initial pressures up to 30 atmospheres. The temperature of the device was demonstrated to be uniform, while the mixture equivalence ratio can be controlled to within 2%, verified using gas chromatograph analysis.

Using a nonlinear extrapolation expression, the laminar flame speed for *n*-pentane/air mixtures was determined at pressures of 1, 2, 5, and 10 atmospheres and  $T_u = 80^\circ\text{C}$ . The Markstein lengths for these mixtures were also reported.

Flames displayed cellular instabilities at high pressures and the radius at which the instabilities formed was measured. These measurements were non-dimensionalized in the form of a Péclet number, showing the expected trend.

A comparison was made with the chemical kinetic mechanism JetSurf0.2. The mechanism was seen to predict flame speeds fairly close to the experimental values with the agreement increasing with increasing pressure.

## 8. Acknowledgments

This research was supported by the Air Force Office of Scientific Research under the technical monitoring of Dr. Julian M. Tishkoff.

### A. Extrapolation of the Laminar Flame Speed

For outwardly propagating flames, the burned gas is assumed to be motionless when the flame is far from the walls of the chamber. Therefore, the downstream or burned flame speed is the rate of change of the flame radius with respect to time,  $s_b = dr_f/dt$ .

The flame speeds measured are subject to stretch effects which are induced, in general, by local flow straining, flame curvature, and flame unsteadiness [28, 29]. Therefore, these effects must be subtracted from the experimental data in order to unambiguously determine the laminar flame speed. Based on asymptotic analysis [30], Wu and Law [31] subtracted the stretch effect by linearly extrapolating the experimental stretched flame speed, determined as a function of the stretch rate, to zero stretch rate according to,

$$\tilde{s} = s - \sigma \quad (2)$$

where  $\tilde{s} = s/s^o$ ,  $\sigma = L\kappa/s^o$  is a non-dimensional parameter,  $s$  the flame speed,  $\kappa$  the stretch rate,  $L$  a constant that measures the mixture's sensitivity to stretch and is commonly referred to as the Markstein length, and the superscript  $o$  refers to the unstretched state. This linear extrapolation has been extensively adopted for flame speed determinations using the counterflow/stagnation flame [32] and the outwardly propagating flame [15, 33]; the references cited are just representative of the many works that have since appeared.

Inherent in the use of Eq. 2 is the assumption that the stretched flame speed does not deviate significantly from the unstretched value. For flames with significantly large Markstein lengths or flames subjected to high stretch rates, the linear relationship between stretch and flame speed does not hold. High molecular weight fuels tend to have relatively large values for their Markstein lengths because of their relatively small mass diffusivities. Additionally, outwardly propagating flame experiments tend to have relatively high values of the stretch rate. This results in measured, stretched, flame speeds that deviate significantly from their unstretched value.

Ronney and Sivashinsky [34] derived an evolution equation for an outwardly propagating flame that does not assume such a linear relation. If we additionally restrict their analysis to flames that are adiabatic and propagate in a quasi-steady manner, the evolution equation for the propagation speed is given by,

$$\left(\frac{s_b}{s_b^o}\right)^2 \ln\left(\frac{s_b}{s_b^o}\right) = -2\frac{L_b\kappa}{s_b^o} \quad (3)$$

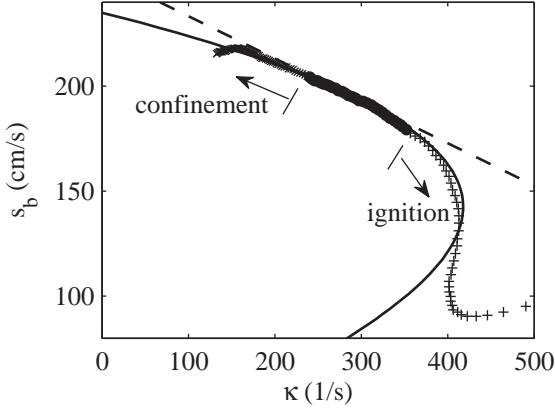


Figure 11: Example experimental data for  $T_u = 298\text{K}$ ,  $\phi = 0.90$ ,  $n$ -pentane/air experiment. Linear extrapolation using Eq. 2 shown as dashed line, nonlinear extrapolation using Eq. 3 shown as solid line.

where we have defined a Markstein length as,

$$L_b = -\frac{1}{2} \frac{E_a}{R^o T_b^o} \ell_T^o I(Le, T_u/T_b^o) \quad (4)$$

and where,

$$I(Le, \epsilon) = \int_{\epsilon}^1 \frac{1}{x} \left[ \left( \frac{x-\epsilon}{1-\epsilon} \right)^{Le-1} - 1 \right] dx \quad (5)$$

$\ell_T^o$  is the unstretched flame thickness,  $E_a$  the activation energy of the one-step global chemical reaction,  $R^o$  the universal gas constant,  $T_u$  the unburned gas temperature, and  $T_b^o$  the adiabatic flame temperature. For outwardly propagating flames, the stretch rate is defined as  $\kappa = (2/r_f) dr_f/dt$ . We see that Eq. 3 reduces to the familiar Eq. 2 in the limit of small deviation of the stretched flame speed from the unstretched value.

While Eq. 3 is the fundamental relation used for the nonlinear extrapolation, fitting of the experimental data and hence the determination of the flame parameters can be conducted more directly by using the raw data for the instantaneous flame radius as a function of time,  $r_f(t)$ , instead of performing numerical differentiation to yield  $s_b$  and  $\kappa$  first. Thus by integrating 3 we have,

$$t = A \left[ E_1(\ln \xi^2) - \frac{1}{\xi^2 \ln \xi} \right] + C \quad (6)$$

where

$$A = \frac{2L_b}{s_b^o}, \quad r_f = -\frac{2L_b}{\xi \ln \xi}, \quad E_1(x) = \int_x^\infty \frac{e^{-z}}{z} dz. \quad (7)$$

Upon successful extrapolation to determine the unstretched downstream flame speed, the upstream flame speed may be determined by use of the continuity equation and thus, the density ratio of the unburned gas to the burned gas,  $s_u^o = s_b^o(\rho_b/\rho_u)$ .

## B. Data for Extrapolation

Care must be taken when choosing data for extrapolation purposes. Figure 11 shows experimental measurements of the stretched flame speed as a function of stretch rate for a typical lean  $n$ -pentane/air experiment at  $\phi = 0.90$ ,  $T_u = 298\text{K}$ , and initial pressure of 1 atm. We have plotted flame speed as a function of stretch as this is the plot typically used for the linear extrapolation using Eq. 2. It is however noted that, as discussed in Appendix A, all extrapolations were performed using the experimentally measured flame radius as a function of time instead of the numerically differentiated quantities of stretch and flame speed.

### B.0.1. Ignition-affected, early-stage flame propagation

Upon spark ignition, the flame is initially driven by thermal conduction from the ignition kernel to the reaction front, resulting in an elevated flame speed. The flame speed subsequently decreases rapidly as the influence of the ignition kernel is dissipated [13]. Following this ignition-dominated phase, the flame speed increases rapidly and this causes the stretch to increase as well, in spite of the simultaneous increase in the flame radius. This early stage propagation may be seen in Fig. 11 as the plus signs at high stretch rates.

To assess the influence of the ignition kernel on the subsequent flame evolution, experiments were conducted with varying spark energy. It was found that the flame may be driven beyond the turning point by excessively large spark energies. However, for low values of the spark energy, the influence of the ignition kernel could be seen to dissipate and experimental results agree before the turning point shown in Fig. 11. Therefore, the highly stretched data occurring before the turning point should not be used due to the possible influence of the ignition kernel. Additionally, Chen *et al.* [22] has shown that the quasi-steady assumption inherent in Eqns. 2 and 3 may be violated up to and slightly beyond the turning point seen in Fig. 11. Therefore we have discarded the data shown as plus signs in Fig. 11 to minimize the influences of the ignition kernel and the transient evolution of the initial flame propagation. It was found experimentally that this corresponded to a radius of approximately 1.0 cm for the  $n$ -pentane flames shown. Therefore, only data with a radius larger than approximately 1.0 cm was used for extrapolation purposes.

### B.0.2. Quasi-steady propagation

During the second period of the flame evolution, the flame speed increases while the stretch rate decreases, indicating that the continuously increasing flame size finally dominates the stretch rate experienced by the flame, exhibiting the conventionally expected behavior that the stretch rate of the flame decreases as it expands.

Data from this phase of propagation vary relatively slowly and hence can be considered to be quasi-steady. The influences of the ignition energy have been dissipated as discussed. Furthermore, the flow field of the unburned gas is unaffected by the confining walls of the chamber, to be substantiated next. The data in this region are shown in Fig. 11 as filled circles.

This region is considered the only region valid for extrapolation purposes.

### B.0.3. Confined, late-stage propagation

During the third period of the flame evolution, the flame speed decreases which, together with the increasing flame radius, cause the stretch rate to decrease. The flame is now fairly large and its propagation can be affected by the confining nature of the inner chamber walls, even though the inner chamber gas is connected to the outer chamber inert gas [23, 35, 36]. Since at this stage the flame is still sufficiently far away from the wall in terms of its thermal thickness, influences that are fluid mechanical in nature due to the restriction of the flow of the un-reacted gas, instead of through conductive heat loss, are expected to be the mechanism in effecting the observed reduction. Furthermore, it was suggested [23, 36] that because of the asymmetrical dimension of the cylindrical chamber, with the radius of the inner chamber being smaller than its length for the present design, the flame propagation velocity will increase in the axial direction and decrease in the radial direction. This could explain the slowing down of the measured flame speed because the flame images recorded were the radial ones, taken along the axial direction.

To assess this influence, experiments were compared on the current apparatus with similar experiments on our previous apparatus. The two experimental configurations primarily differ in the geometry of the inner chamber with the current chamber having a length of 5 inches and an inner diameter of 4.5 inches, while the previous design had the same length, but a smaller inner diameter of 3.25 inches.

Figure 12 shows experimental results obtained from these two geometrically distinct chambers, with the open and closed symbols respectively designating the smaller and larger inner diameter chambers. We see that the flame responses initially differ due to the slight difference in the ignition energy, but they quickly merge. Subsequent to the turning point, the flames quasi-steadily propagate free of the ignition energy influence and their responses agree well. However, upon reaching a large radius and correspondingly small stretch rate, the two flames evolve differently, with the flame in the smaller inner diameter chamber slowing down, while the flame in the larger diameter inner chamber continues with the apparently quasi-steady propagation. The point at which the two experiments begin to diverge identifies the stage at which the chamber geometry starts to influence the flow field of the unburned gas such that data beyond this stage for the smaller chamber should not be used for extrapolation purposes.

Additional experiments were performed with the current apparatus which varied the locations of the holes that connected the inner and outer chambers and similar results were obtained as those shown in Fig. 12, with experiments agreeing until reaching a large radius at which stage the hole locations, and thus the geometry of confinement, begin influencing the flame propagation and motion of the unburned gases. Based on the above results, we have determined that, for typical *n*-pentane/air experiments using our current experimental setup, the radius at which the chamber walls and hole locations began influencing

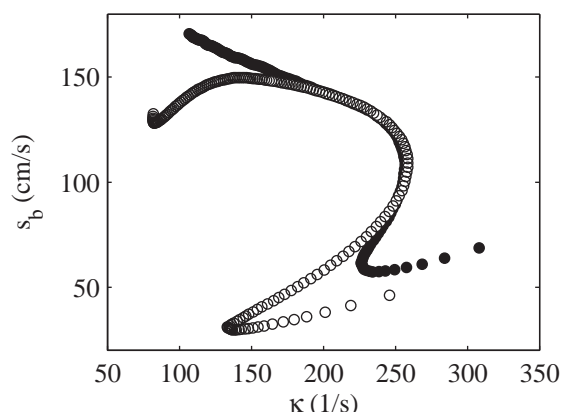


Figure 12: Example experimental data for n-butane/air experiments with  $T_u = 298\text{K}$ ,  $\phi = 0.80$ , at 1 atm initial pressure. Comparison is shown between two geometrically distinct inner chambers: open circles – I.D. 3.25 inches, closed circles – I.D. 4.5 inches

the propagation was approximately 1.8 cm. Therefore, all data with flame radius larger than 1.8 centimeters were not used for the extrapolation of the laminar flame speed.

### B.1. Data range for extrapolation

Similar experiments as described above were conducted with rich *n*-pentane/air mixtures to determine the influences of ignition energy and confinement and were found to have similar experimental limitations. Therefore, the data used for regression was typically taken between a radius of 1.0 cm to 1.8 cm for all experiments. This conservative range allows accurate extrapolations while removing the influence of the ignition transient and the influence of the chamber boundary.

## References

- [1] B. Sirjean, E. Dames, D. A. Sheen, X.-Q. You, C. Sung, A. T. Holley, F. N. Egolfopoulos, H. Wang, S. S. Vasu, D. F. Davidson, R. K. Hanson, H. Pitsch, C. T. Bowman, A. P. Kelley, C. K. Law, W. Tsang, N. P. Cernansky, D. L. Miller, A. Violi, R. P. Lindstedt, A high-temperature chemical kinetic model of n-alkane oxidation, JetSurF version 0.2, [http://melchior.usc.edu/JetSurF/Version0 2/Index.html](http://melchior.usc.edu/JetSurF/Version0%20Index.html) (September 2008).
- [2] S. G. Davis, C. K. Law, Laminar flame speeds and oxidation kinetics of iso-octane-air and n-heptane-air flames, Proceedings of the Combustion Institute 27 (1998) 521–527.
- [3] S. G. Davis, An experimental and kinetic modeling study of the pyrolysis and oxidation of selected C<sub>3</sub>–C<sub>8</sub> hydrocarbons, Ph.D. thesis, Princeton University, Department of Mechanical and Aerospace Engineering (1998).
- [4] S. G. Davis, C. K. Law, Laminar flame speeds and oxidation kinetics of benzene/air and toluene/air flames, Proceedings of the Combustion Institute 26 (1996) 1025–1033.
- [5] S. G. Davis, C. K. Law, Determination of and fuel structure effects on laminar flame speeds of C<sub>1</sub> to C<sub>8</sub> hydrocarbons, Combustion Science and Technology 140 (1999) 427–449.
- [6] C. Ji, A. T. Holley, F. Egolfopoulos, X. You, E. Dames, B. Sirjean, H. Wang, Flame studies of jet fuels and surrogate-related neat components, Multi-Agency Coordination Committee for Combustion Research (MACCCR) Summit on Fuels.
- [7] C. K. Law, Combustion Physics, Cambridge University Press, 2006.

- [8] A. J. Smallbone, W. Liu, C. K. Law, X. Q. You, H. Wang, Experimental and modeling study of laminar flame speed and non-premixed counterflow ignition of *n*-heptane, *Proceedings of the Combustion Institute* 32 (2009) 1245–1252.
- [9] D. Bradley, R. A. Hicks, M. Lawes, C. G. W. Sheppard, R. Woolley, The measurement of laminar burning velocities and Markstein numbers for iso-octane-air and iso-octane-*n*-heptane-air mixtures at elevated temperatures and pressure in an explosion bomb, *Combustion and Flame* 115 (1998) 126–144.
- [10] S. Jerzembeck, N. Peters, P. Pepiot-Desjardins, H. Pitsch, Laminar burning velocities at high pressure for primary reference fuels and gasoline: Experimental and numerical investigation, *Combustion and Flame* 156 (2009) 273–291.
- [11] A. Al-Shahrany, D. Bradley, M. Lawes, R. Woolley, Measurement of unstable burning velocities of iso-octane-air mixtures at high pressure and the derivation of laminar burning velocities, *Proceedings of the Combustion Institute* 30 (2005) 225–232.
- [12] R. Johnstone, J. Farrell, Laminar burning velocities and Markstein lengths of aromatics at elevated temperature and pressure, *Proceedings of the Combustion Institute* 30 (2005) 217–224.
- [13] A. P. Kelley, G. Jomaas, C. K. Law, Critical radius for sustained propagation of spark-ignited spherical flames, *Combustion and Flame*.
- [14] G. Jomaas, X. L. Zheng, D. L. Zhu, C. K. Law, Experimental determination of counterflow ignition temperatures and laminar flame speeds of C<sub>2</sub>–C<sub>3</sub> hydrocarbons at atmospheric and elevated pressures, *Proceedings of the Combustion Institute* 30 (2005) 193–200.
- [15] G. Rozenchan, D. L. Zhu, C. K. Law, S. D. Tse, Outward propagation, burning velocities, and chemical effects of methane flames up to 60 atm, *Proceedings of the Combustion Institute* 29 (2002) 1461–1469.
- [16] G. Rozenchan, An experimental study of outwardly propagating hydrogen and methane flames at high pressures, Ph.D. thesis, Princeton University, Department of Mechanical and Aerospace Engineering (2001).
- [17] S. D. Tse, D. Zhu, C. K. Law, Morphology and burning rates of expanding spherical flames in H<sub>2</sub>/O<sub>2</sub>/inert mixtures up to 60 atmospheres, *Proceedings of the Combustion Institute* 28 (2000) 1793–1800.
- [18] X. Qin, Y. Ju, Measurements of burning velocities of dimethyl ether and air premixed flames at elevated pressures, *Proceedings of the Combustion Institute* 30 (2005) 233–240.
- [19] X. J. Gu, M. Z. Haq, M. Lawes, R. Woolley, Laminar burning velocity and Markstein lengths of methane-air mixtures, *Combustion and Flame* 121 (2000) 41–58.
- [20] J. de Vries, B. A. Corbin, E. L. Petersen, A facility for high-pressure laminar flame speed measurements, 5th U.S. Combustion Meeting.
- [21] S. D. Tse, D. Zhu, C. K. Law, Optically accessible high-pressure combustion apparatus, *Review of Scientific Instruments* 75 (2004) 233–239.
- [22] Z. Chen, M. P. Burke, Y. Ju, Effects of Lewis number and ignition energy on the determination of laminar flame speed using propagating spherical flames, *Proceedings of the Combustion Institute* 32 (2009) 1253–1260.
- [23] M. P. Burke, Y. Ju, F. L. Dryer, Effect of flow field perturbations on laminar flame speed determination using spherical flames, 46th AIAA Aerospace Sciences Meeting and Exhibit.
- [24] A. P. Kelley, C. K. Law, Nonlinear effects in the experimental determination of laminar flame properties from stretched flames, Meeting of the Eastern Section of the Combustion Institute.
- [25] G. Jomaas, C. K. Law, J. K. Bechtold, On transition to cellularity in expanding spherical flames, *Journal of Fluid Mechanics* 583 (2007) 1–26.
- [26] J. K. Bechtold, M. Matalon, Hydrodynamic and diffusion effects on the stability of spherically expanding flames, *Combustion and Flame* 67 (1987) 77–90.
- [27] C. J. Sun, C. J. Sung, L. He, C. K. Law, Dynamics of weakly stretched flames: Quantitative description and extraction of global flame parameters, *Combustion and Flame* 118 (1999) 108–128.
- [28] F. A. Williams, A review of some theoretical considerations of turbulent flame structure, AGARD Conference Proceedings 164.
- [29] M. Matalon, On flame stretch, *Combustion Science and Technology* 31 (1983) 169–181.
- [30] M. Matalon, B. J. Matkowsky, Flames as gasdynamic discontinuities, *Journal of Fluid Mechanics* 124 (1982) 239–259.
- [31] C. K. Wu, C. K. Law, On the determination of laminar flame speeds from stretched flames, Twentieth Symposium (International) on Combustion (1984) 1941–1949.
- [32] D. L. Zhu, F. N. Egolfopoulos, C. K. Law, Experimental and numerical determination of laminar flame speed of methane/(Ar N<sub>2</sub>CO<sub>2</sub>)-air mixtures as function of stoichiometry, pressure, and flame temperature, Twenty-Second Symposium (International) on Combustion 22 (1988) 1537–1545.
- [33] D. R. Dowdy, D. B. Smith, S. C. Taylor, A. Williams, The use of expanding spherical flames to determine burning velocities and stretch effects in hydrogen/air mixtures, Twenty-Third Symposium (International) on Combustion (1990) 325–332.
- [34] P. D. Ronney, G. I. Sivashinsky, A theoretical study of propagation and extinction of nonsteady spherical flame fronts, *SIAM Journal on Applied Mathematics* 49 (4) (1989) 1029–1046.
- [35] M. P. Burke, X. Qin, Y. Ju, F. L. Dryer, Measurements of hydrogen syngas flame speeds at elevated pressures, 5th U.S. Combustion Meeting.
- [36] M. P. Burke, Y. Ju, F. L. Dryer, Effect of cylindrical confinement on the evolution of outwardly propagating flames, Meeting of the Eastern States Section of the Combustion Institute.